Structural Conservation of Insulin/IGF Signalling Axis at the Insulin Receptors Level in *Drosophila* and Humans

Cristina M. Viola[1,5], Orsolya Frittmann[1,2], Huw T. Jenkins[1], Talha Shafi[1], Pierre De Meyts[3,4] & Andrzej M. Brzozowski[1*]

[1] York Structural Biology Laboratory, Department of Chemistry, University of York, Heslington, York YO10 5DD, United Kingdom

[2] Current address: Department of Haematology, University Medical Center Groningen, , Hanzeplein 1, 9713 GZ Groningen, Netherlands

[3] Department of Cell Signalling, de Duve Institute, B-1200 Brusssels, Belgium.

[4] Department of Cell Therapy Research, Novo Nordisk A/S, DK-2670 Maaloev, Denmark.

[5] Current address: Department of Biology, University of York, Heslington, York YO10 5DD, United Kingdom

*corresponding author: marek.brzozowski@york.ac.uk, phone: +441904328265, fax: +441904328266, ORCID ID: 0000-0001-7426-8948

Keywords: insulin, IGF-1, DILP5, DILP, Insulin Receptor, IGF-1R, insulin signalling axis, *Drosophila*

ABSTRACT

The family of insulin-related hormones regulates key life processes in Metazoa, from metabolism to growth, reproduction, lifespan and aging, through an evolutionarily conserved Insulin/insulin-like growth factor-1 (IGF-1) signalling (IIS) axis. In humans the IIS axis is controlled by insulin, two insulin-like growth factors, two isoforms of the insulin receptor (hIR-A and -B), its homologous IGF-1R and their hybrid dimers. In *Drosophila*, this signalling engages seven insulin-like proteins (DILP1-7) and a single receptor (dmIR), with many downstream proteins and pathways that are homologous with human ones. This report reveals the first cryoEM structure of the dmIR ectodomain:DILP5 complex providing the evidence of structural homology between dmIR and hIR. In the presence of excess hormone, the overall organisation of the dmIR complex is an asymmetric '*T*' conformation, similar to that observed in some human IR structures. However, dmIR binds three DILP5 molecules in an unseen arrangement, revealing unique structural signatures that could rationalize the selective binding and signalling by different DILPs. This work provides structural proof of the evolutionary conservation of key receptors of the insulin-like hormones signalling axis, underpinning a deeper understanding of an important model animal organism.

INTRODUCTION

The insulin/insulin-like growth factor signalling axis (IIS) is an evolutionarily ancient, highly conserved, endocrine and paracrine signal transduction network in Metazoa (Chan & Steiner, 2000; De Meyts, 2004) . It regulates a broad spectrum of key life processes such as metabolism, growth, development, reproduction, aging and lifespan, and cell growth, differentiation and migration at the cellular level.

In humans and many vertebrates, insulin is stored in oligomeric crystalline forms in pancreatic β-cells and is acutely secreted into the circulation in monomeric form in response to glucose and nutrients (Weiss *et al,* 2014), while its homologous human Insulin-like Growth Factors (hIGF-1 and 2) do not aggregate (Brzozowski *et al,* 2002) and are secreted by multiple tissues as monomers, being tightly bound in biological fluids by several IGF Binding Proteins (IGFBP1-6) (Forbes *et al.,* 2012). Ultimately, insulin and IGFs transduce their signals through closely related cell-surface tyrosine kinase type (RTK) insulin and IGF-1 receptors, and through their hybrid dimers (Adams *et al,* 2000; De Meyts & Whittaker, 2002; Denley *et al.,* 2005; Siddle, 2012; De Meyts, 2016; Saltiel, 2021; Nagao *et al.,* 2022) (Fig. **1a**).

The occurrence of similar insulin/IGFs-like hormones - Insulin-like Proteins (ILPs) - is very diverse in the animal kingdom, ranging from 7 ILPs in *Drosophila* (DILP1-7), to 40 ILPs in *Bombyx mori* and *Caenorhabditis elegans* (Adams *et al,* 2000; Brogiolo *et al*, 2001; Grönke *et al,* 2010; Post *et al,* 2018; Pierce *et al,* 2001; Kenyon *et al.,* 2011). . An eighth ILP in *Drosophila* (DILP8) is a paralogue of human relaxin and binds to a G-protein-coupled receptor, Lgr3 (Colombani *et al.,* 2015). All these hormones share similar motifs of inter-/intra-chain disulfide bridges and organisation typical for human insulin, i.e. two chains named A, B with the middle C-domain released from the prohormone, or being retained in certain ILPs, such as human proinsulin and hIGF-1/2 (**Fig. 1b**, **SI Fig. 1**). Despite the variety of the ILPs, in humans they control two isoforms of insulin receptor (hIR-A and -B) and one IGF receptor (hIGF-1R) (Adams *et al.* 2000; De Meyts & Whittaker, 2002). *Drosophila melanogaster* (Dm) and *Caenorhabditis elegans* only encode a single so-called insulin receptor that relays signaling from a plethora of ILPs (Brogiolo *et al,* 2001; Grönke *et al,* 2010; Pierce *et al*, 2001) (**Fig. 1a**). As a result, DmIR is involved in a broad spectrum of life processes including development, regulation of life span, metabolism, stress resistance, reproduction and growth. The recently discovered presence of IR gene duplication and decoy (TK-free) dmIR-framework based receptors in certain insects lineages has been postulated to

play a role in phenotypic plasticity and caste differentiation in insect taxa (Kremer *et al,* 2018; Smýkal *et al,* 2020; Okamoto *et al,* 2022)). Close structural and functional homology between mammalian and invertebrates ILPs and their IRs is illustrated, for example, by the activation of dmIR by human insulin (Petruzelli *et al,* 1985; Sajid *et al,* 2011)), the insulin-like bioactivity of DILP5 in mice and Drosophila (Sajid *et* al, 2011)), and hIR activation (on the functional and structural level) by the cone snail venom insulin (Xiong *et al,* 2022).

Drosophila is a widely used model for many human pathologies ranging from metabolic disorders to neurodegeneration as over 75% of human-disease-related genes are conserved in this animal (Bier, 2005). Over 100 years as a model organism led to the development of a rich pool of versatile loss-of-function and epistasis genetic tools (Ugur *et al,* 2016). The network of IIS axis is reduced in flies, usually by the presence of only one downstream signalling homologue, i.e., a lower redundancy at the signal amplification levels (**Fig. 1a**), a direct comparison of the human and Dm IIS axes remains complex (Teleman *et al,* 2012). For example, a recent structure of the *Drosophila* insulin binding protein Imp-L2 dispelled the commonly held notion that it is a homologue of human IGFBPs but rather represents a very different family of insect proteins involved in the regulation of DILPs bioavailability (Roed *et al,* 2018).

Pioneering biochemical studies in the 70's (Pullen *et al,* 1976; De Meyts *et al,* 1978) established a largely invariant region of human insulin as a good candidate for the receptor-binding epitope (now referred as to site 1), including A-chain residues GlyA1, GlnA5, TyrA19, AsnA21, and B-chain residues ValB12, TyrB16, PheB24, PheB25 and TyrB26. Subsequently, these were extended to SerA12, Leu A13, GluA17, HisB10, GluB13, Glu B17 and Ile A10 (De Meyts, 1994, 2015; De Meyts & Whittaker, 2002), which form insulin receptor binding site 2. Two binding sites equivalent to insulin's sites 1 and 2 have also been identified on IGF-I and II by site-directed mutagenesis (Gauguin *et al,* 2008; Alvino *et al,* 2009), with site 1 extending into their C-domain. The engagement of insulin/IGFs site 1 and 2 in hIR/mIR/IGF-1R binding was ultimately confirmed in the last decade in over 40 crystal and cryoEM structures of complexes of these hormones (as well as insulin mimetic peptides and aptamers) with their cognate receptors and their extensive functional studies (Kavran *et al,* 2014, Croll *et al,* 2016; Weis *et al,* 2018; Xu *et al,* 2018, 2020, 2022; Scapin *et al*, 2018; Gutmann *et al*, 2018, 2020; Uchikawa *et al*, 2019; Li *et al*, 2019, 2022 a&b; Blyth *et* al, 2020; Zhang *et al*, 2020, 2022 a&b; Xiong *et al*, 2022; Nielsen *et al*, 2022; Wu *et al*, 2022;

Kirk *et al*, 2022; Park *et al*, 2022; Kim *et al*, 2022; for reviews, see Lawrence, 2021; Forbes, 2023).

Despite astonishing 3-D insights into the holo- and apo forms of hIR/mIR/hIGF-1R, several key questions about their insulin-binding triggered activation and complex allosteric signal transduction still remain. The variety of insulin:IR stoichiometries with a broad spectrum of conformations of the ectodomains (ECD) of these receptors, led to several alternative models of triggering of the IR signalling by insulin (**Fig. 1c**).

The importance of understanding of *Drosophila* IIS axis contrasts with the lack of any structural description of the dmIR, nor of any other non-mammalian/invertebrate IRs, although there is some extensive mutagenesis-based insight into dmIR tyrosine kinase (Tatar, 2021). This prompted us to undertake the structural characterization of the dmIR ectodomain (dmIR-ECD) in its apo- and holo-form in the complex with the *Drosophila* DILP5 hormone.

The dmIR primary structure, with ~33% sequence identity in the overlapping regions (Fernandez *et* al, 1995; Ruan *et al,* 1995), indicates that it should share the same domain organisation as all IRs-like receptors (hIR, IGF-1R, mice IR (mIR)) (**SI Fig. 2**). They are unique homodimers with an $(\alpha\beta)_2$ subunit organisation, having the same modular, exons-reflecting organisation (**Fig. 1d**). In hIR the α-subunits consist of L1 (Leucine-rich repeats domain 1), CR (Cysteine Rich), L2, FnIII-1 (Fibronectin type III-like), FnIII-2 and internally spliced ID (Insert domain) modules. The β-subunit starts with the remaining parts of the spliced ID and FnIII-2 domains that are followed by the FnIII-3 domain, the transmembrane helix (TM), juxtamembrane (JM) and TK modules (De Meyts & Whittaker, 2002). Both α-subunits are linked by structurally and functionally important SS bonds (Adams *et al,* 2000).

The L1 domain and the crossing-over α–CT' terminal region of the ID' domain from the other α-subunit form the so-called main, high affinity insulin binding site 1 (and 1') (e.g., L1/α–CT', L1'/α–CT) (the (') denotes contribution from the other symmetrical αβ half of the IR) (Menting *et al*, 2013). The α–CT' segments lie across the L1β2 sheet of the L1 domain, shifting their positing there towards the ultimate mediation of a mostly indirect tethering of insulin to the L1β2 surface. The so-called insulin low-affinity sites 2 (and 2') are on surfaces of the FnIII-1 (FnIII-1') domains (Lawrence, 2021; Forbes, 2023). The dmIR ends with a unique 60 kDa extension: C-terminal domain (CTD), with its N-terminal part having 22% sequence identity with human intracellular Insulin Receptor Substrate 1 (Fernandez *et al*, 1995; Ruan *et al,* 1995) (IRS1)(**Fig. 1d, SI Fig. 2**).

Human IR (and mIR) structures consistently revealed the apo-IR in an inverted V - Λ-like - form, and its very opposite - fully insulin saturated – symmetrical T-shaped form with two insulins in each of the sites 1/1' and sites 2/2' (reviewed in Lawrence, 2021; Forbes, 2023). Many 'intermediate' hIR/mIR structures have been found between these two extreme IR conformers, with one, two, or three insulins bound (Nielsen *et al,* 2022; Forbes, 2023). These intermediate structures show show the α-arms of the receptor in many asymmetrical *Γ* and *T* conformations, from one arm-down/one-up, with the different stages of detachment of the down-arm from the FnIII-1 – FnIII-3-stem of the receptor (Fig. **1c**)(Forbes, 2023). It seems that the disulphide(s)-connected ID and ID' linkers that end with the helical α–CT segments correlate the movement of these helices (and other parts of the IR) upon insulin binding into complex allosteric effects within the IR (Li *et al,* 2022b)). The αβ half of the IR with the up-arm and site 1 bound insulin has also been referred as the so-called static 'invariant' protomer, as it does not deviate significantly in IR-holo forms, while the down-arm of the other αβ half - in different stages of the detachment form the stem of the receptor - is described as a dynamic protomer. There is no single explanation of the activation steps of the hIR/mIR yet, but it can be envisaged that binding of insulin to one low-affinity site 2 triggers the sequence of allosteric effects leading to successive association(s) of the hormone with high-affinity site(s) 1 (Nielsen *et* al, 2022; Forbes, 2023).

We selected the *Drosophila* DILP5 for dmIR-ECD studies as a typical representative and well characterized fly ILP, having also a high homology to human insulin (~28% sequence identity) (Sajid *et* al, 2011, **SI Fig. 1**), and with nM-range K_d for the dmIR high affinity site 1 of 0.76 (+/-0.16) nM (Sajid *et al,* 2011) that is within a range of human insulin:hIR interaction (e.g., 0.2-0.7 nM)(Kiselyov *et al,*). Each of the DILP1-7 has a unique expression pattern and regulation, with DILP5 being expressed in neurosecretory cells of the *Drosophila* brain, midgut and ovaries, and the ablation of these cells reflects the reduction of insulin signalling in mammals, e.g., leading to whole-body increase of trehalose in the fly (Teleman *et al,* 2012; Sajid *et al,* 2011).

The only structural-functional insight into DILP5 are crystal structures of this hormone studied along its IRs binding properties (Sajid *et al,* 2011), and of DILP5 complex with Dm Insulin Binding Protein Imp-L2 that is involved in the regulation of DILP5 bioavailability (Roed *et al,* 2018). These studies revealed evolutionary structural and functional conservation of DILP5, with its very human insulin-like structure, and with substantial hIR affinity (K_d ~60 nM).

Here, we provide the first 3-D description of an invertebrate IR-like receptor by determining the cryoEM apo and holo structures of the dmIR-ECD. For the complex, the DILP5 C4 variant of this hormone (referred here to as DILP5) was used (Sajid *et al,* 2011) (**SI Fig. 1**). It has an AspA1-PheA2-ArgA3 A-chain extension in comparison with so-called DILP5 DB variant; they have been studied with their alternative A-chain sequence due to the ambiguity about their *in vivo* cleavage and processing sites (Sajid *et al*, 2011).

This report provides the first structural evidence of the conservation of the IIS axis in the animal kingdom at the IR level, where dmIR-ECD follows remarkably the principle and organisation of human and mice IRs. However, a handful of dmIR-ECD unique features are shedding light on a possible adaptation of this system for *Drosophila*-specific multi-hormone driven signal transduction through this receptor.

RESULTS

General organisation of the dmIR-ECD.

The apo-form of the dmIR has only been outlined here at a very low resolution as its molecules constituted only a small sub-fraction of the observed particles (**SI Fig. 3**). Nevertheless, the conformations of hIRs and dmIR-ECD apo forms are similar, appearing as Λ-like intertwined $(\alpha\beta)_2$ homodimers. They likely represent the non-signalling forms of the receptor due to a large separation (~110 Å) of its FnIII-3 domains, and, subsequently, intra-cellular TK domains.

The holo-dmIR-ECD has been obtained with 5:1 hormone:IR ratio which resulted in a unique asymmetric three-insulins:IR complex with two adjacent insulins bound to sites 1 and site 2' on the arm-down/dynamic and static protomers, respectively, and one insulin at site 1' on the arm-up/static protomer (**Fig. 2**). Such IR conformer has not been seen in any wild type human insulin:IR complex, where if three-insulins:hIR complex was observed there was a clear separation between site 1 and site 2' bound hormones (e.g., PDB ID 7PG0, (Nielsen *et* al, 2022).

Despite a large phylogenetic gap between humans and insects, the principles of the overall 3-D organisations of h(m)IR/hIGF-1R and dmIR ECDs are very similar, revealing the evolutionary conservation of the IIS signalling axis at the receptor level (Adams *et* al, 2000; De Meyts, 2004, **Fig. 1a**). The structure of the dmIR-ECD $(\alpha\beta)_2$ homodimer follows closely the multidomain order and size of hIR/hIGF-1R ectodomains (hIR-ECD/IGF-1R-ECD) (**Fig. 1d, SI Fig. 2**). As dmIR-ECD is similar to both hIR and hIGF-1R ECDs, and this report

concerns dmIR-ECD complex with more human insulin-like DILP5, rather than with a single-chain IGFs-like hormone, the comparison focus here of dmIR and hIR for the brevity the analysis; the structural trends observed here are practically mirrored in the hIGF-1R. However, it should be noted that the hIGF-1R also remains asymmetrical with only one IGF-1 molecule bound to site 1 even in the presence of a large excess of ligand (Li *et* al, 2019). This phenomenon can be linked to so-called negative cooperativity within the family of the IR-like receptors (De Meyts *et al,* 1973; De Meyts, 1994) that is addressed in the Discussion.

The dmIR-ECD αβ protomers follows the same L1-CR-L2-FnIII-1-FnIII-2-ID (α subunit) and ID-FnIII-2-FnIII-3 (β subunit) domains organisation as in h(m)IRs/hIGF-1R. This analogous blueprints are underpinned by a remarkable 3-D structural similarity of the individual domains of these receptors. The pairwise root mean square deviations (rms) between structures of the respective domains of the reported hIR/hIGF-1R and dmIR ECDs are rather small for the Cα atoms, mostly within the range of 0.80-2.15 Å (**SI Table 2**). However, dmIR-ECD shows several unique structural signatures - unique loops - that shed some light on how dmIR may handle signalling that involves seven DILPs through only one 'universal' IR (see further below).

The only significant deviation from the hIR fold is the large ~Gly491-Cys512 insert into the first part of the CR domain. However, this peripheral loop - very disordered and not accountable in the cryoEM density map (modelled here for just noting its presence) - is not directly involved in any hormone binding hence its role is unclear. It cannot be excluded though that it is involved in a firmer attachment of the L1 domain to the dmIR protomers in the apo-dmIR, or, just opposite, it prevents a fully-down conformation of the L1-CR-L2 arm of hormone-free protomer (Weiss *et al,* 2014), by its potential clashes with the FnIII-3' domain (**SI Fig. 4**).

Overall mode of DILP5 – dmIR-ECD binding.

Despite a unique distribution of insulins in three-DILP5:dmIR complex this asymmetric arm-down(Λ):arm-up(*Γ*) remains within range of some known hIR asymmetric *T* conformers (e.g. PDB 7PG0, 7PG2, 7PG4 (Nielsen *et* al, 2022) – see end of the Results). The overall binding modes of site 1 (down-arm (Λ) and 1' up-arm site 1' (*Γ*)) follows closely respective human insulin complexes (**Fig. 2ab**). However, the third DILP5 molecule engages site 2' on the FnIII-1' domain of the static protomer, being adjacent to and in contacts with the down-arm site 1-bound DILP5, while the site 2 is unoccupied **(Fig. 2c, Fig. 3b**). Such asymmetric

insulin binding to the hIR was postulated as structurally unfeasible due to envisaged steric clashes between hormone molecules occupying simultaneously lower/dynamic-arm based site1 and static protomer site2' (Li *et al,* 2022). Therefore this two-hormones-down and one-hormone up *T* asymmetric conformation of the DILP5:dmIR complex can be considered as a specific signalling form of the dmIR, especially as the supersaturated insulin:receptor conditions used yielded only T symmetrical hIR conformers (e.g., PDB SOF, 6PXW/6PXV) (Gutmann *et al,* 2020; Uchikawa *et al,* 2019).

The conservation and uniqueness of sites 1/1' and 2/2' in dmIR-ECD.

The structural principles of DILP5 engagement with L1/α-CT sites 1 are very similar to the human insulin:site1 complexes with very low rms for both down- (~0.9-1.4 Å) and up-L1 (~1.1 – 2.0) domains, and respective helical parts of the α-CT segments (~0.8 Å) when compared with their human IR (or hIGF-1R) counterparts (**SI Table 1**).

The overall fold of the FnIII-1 domains - the main components of site 2 and 2' – is also very similar in dmIR-ECD and hIR (~1.2 – 1.9 rms range), and the mode of DILP5:site 2' interaction is - in principle - similar in both receptors. However, DILP5 sits ~6 Å lower on FnIII-1' side-surface than insulin in hIR's sites 2, with its B-helix also closer by ~2.7 Å to FnIII-1', especially when compared at the Cα atoms of ValB16(LeuB17) at sites 2 in the hIR (corresponding hIR (or insulin) sequences are given in brackets) **(Fig. 3c).** This lowering of site 2' in dmIR is likely needed for the simultaneous accommodation of both DILP5s in site 1 and site 2' in the lower-arm environment. This unique proximity of both site 1/site 2'-bound hormones may be facilitated further by a shorter Lys884-Gly886 loop in the dmIR (Pro536-Pro539 in hIR), and much longer in the dmIR Ala1168-Ser1189 loop (Ala785-Ser796) from the FnIII-2' domain that becomes now an integral part of site 2' **(Fig. 3cd**). Here, the shorter Lys884-Gly886 FnIII-1 loop minimises steric hindrance upon binding of both DILP5s into the lower arm site1/2' space, while the longer – dmIR specific - Ala1168-Ser1189 loop (with central short Ile1173-Thr1181 helix) provides a supporting ledge for the site 2' DILP5. This FnIII-2' ledge seems to be stabilised by the internal Arg1170-Glu1176 salt-bridge, and Cys1169-Cyss1188 (Cys786-795) SS bridge at the base of the ledge gives further solidity to this region, while ledge's Phe1183 serves a hydrophobic platform for DILP5 MetB11 (**Fig. 3d**). This contrasts with hIR where none of the FnIII-2 domains contribute to site 2/2'.

A close up on both site 1 DILP5 binding modes reveals a similar pattern of the interactions in its 'classical' 1a subsite (Uchikawa *et al,* 2019) which involves L1-β2-surface:α-CT':hormone interfaces . The helical α-CT' segment provides the same in-between anchoring base for DILP5 running relatively perpendicularly to the strands of the L1-β2 sheet, as observed in hIR (**Fig**. **3ef**). Structural conservation in site 1a/1a' binding of DILP5 and human insulins is also reflected in maintaining the chemistry and role of the key amino acids on the main hormone:IR interaction surfaces. For example, this can be seen on the: (i) L1-β2:α-CT' surface – Leu368(Leu37), Phe416(Phe88), Tyr419(Tyr91), Val422(Val94), Arg446(Arg118), Glu448(Glu120), (ii) on the L1-β2:DILP5 interface – Asp343(Asp12), Asn346(Asn15), Ley368(Leu37), Arg343(Arg65), (iii) and on the αCT':DILP5 interface – Phe1035(Phe705), Glu1036(Glu706), Leu1039(Leu709), Asn711(Asn1041), Phe1044(Phe714), Val1045(Val715). Such conservation applies also to the DILP5 surfaces involved in binding to site 1a/1a': GlyA4(GlyA1), ValA5(IleuA2), ValA6(ValA3), AspA7(GluA4), TyrA22(TyrA19), AspA14(Asn21), PheB22(PheB24).

Nevertheless, the divergence of both hormone/receptor sequences have structural and (likely) functional impacts on some important parts on the hormone:receptor site 1a/1a' interfaces. For example, DILP5 (and DILP1) specific ProB19 replacement of human GlyB20, and deletion of the equivalent of human ArgB22, pushes the DILP5 B20-B26 chain closer to the L1-β2 surface in proline's more 'stereo-specific'-like fashion (**Fig**. **4ab**). Still, the conserved PheB22(PheB24) side chain is wedged into the hydrophobic cavity of PheI15(Phe714), Leu368(Leu37), LeuB14(LeuB15), CysB18(CysB19)-CysA23(CysA20), similarly to the human hormone, and, remarkably, the B22(B24) phenyl rings occupy the same space in both complexes (**Fig**. **4ab**). Although, the B23-B28 chain of DILP5, different from the human sequence, makes more dmIR-specific local interactions, it still follows the overall direction of this peptide across the L1-β2 surface observed in human complexes. This, subsequently, allows MetB25 – equivalent to the important human site 1a TyrB26 – to be engaged in the Phe603, Val1045, Phe1042 hydrophobic cavity, along the TyrB26 structural role in human complexes **(Fig. 4b).**

The preservation of such key contacts is propagated locally and globally onto other structural interfaces in dmIR-ECD and human IRs. For example, α-CT' Phe1035(Phe705) is wedged into a hydrophobic cavity made by L1-β2 and α-CT' amino acids Tyr419(Tyr91), Phe416(Phe88), Leu1039(Leu79), Tyr424(Phe96) (**Fig. 4c**). The environment of Phe1035 is also stabilised by nearby Arg446(Arg118) involved in dmIR-ECD/hIR conserved hydrogen

bonds triad with Tyr419(Tyr91) and Glu448(Glu120) (with potential Arg guanidinium-π-Phe1035(Phe705) interaction as well).

The AspA1-PheA2-ArgA3 extension of the A-chain N-termini in DILP5 C4 variant is readily accommodated in both sites 1. In site 1a (down) it is wedged between the CR-domain Ala594-Asn615 loop and L2 domain, with some HBs such as ArgA3 CO-ND2 Asn606, and ArgA3 NH1 – CO Glu660. As the A1-A3 chain points towards outside of the dmIR, and is not obstructed by the receptor, it seems that the accommodation of DILPs with A-chains N-termini extensions (DILP1, 6, 7) can be easily achieved here (**Fig 4a**). The A1-A4 chain is very extended in site 1a, being more compact - towards a more helical conformation - in site 1a'. Therefore, a shorter N-termini of the A-chain of the DILP5 DB variant may be beneficial for dmIR-binding of this more compact hormone (K_d of 0.35 nM in comparison with 0.76 nM for DILP5 C4 variant (Sajid *et al,* 2011)).

The 1b sub-component of site 1 (Uchikawa *et al,* 2019)), which involves the hormone:FnIII-1 interface, is dissimilar in sites 1b and 1b' due to different exposition of parts of FnIII-1 to DILP5 on the down- and up-arms of the dmIR-ECD. The upper (Γ) arm of the dmIR-ECD static protomer should have, in principle, an overall more classical site 1b' environment but the conservation of human-insect hormone-receptor contacts is rather uneven here due to a different length of corresponding FnIII-1 loops in hIR/hIGF-1R and dmIRs. Here, DILP5' engages its ArgB4(HisB10), AlaB5(LeuB6), CysB6(CysB7)-CysA10(CysA10), ProB8 in site 1b' while FnIII-1 contributes there Lys845, Asp846(Asp496), Pro847, Arg848(Arg498). The other impact on structure of site 1b' comes from dmIR-specific Thr827-Ile842 FnIII-1 domain insertion loop which may dictate conformation of DILPs B1-B6 N-terminus in the static protomer (**Fig**. **3f**). This loop narrows the space for the B1-B6 chain that is close to the DILP5 core in a tight T-like state. The N-terminus of the DILP5 B-chain can be accommodated in the site 1b', but binding of DILPs with B-chain long N-terminal extension, e.g. DILP1 and DILP7 (13 and 23 residues, respectively) can result in a steric hindrance with 827-842 loop. It seems that Pro8(SerB7) can have a particular role here by directing the B1-B7 chain as close as possible to the core of the hormone, to assure its tight fit in-between the hormone and the surface of the receptor. Such close packing of T-form-like B1-B7-chain is observed on all three DILP5:dmIR interfaces.

The site 1b interface on the Λ down-arm is less extensive, reflecting a different DILP5:FnIII-1' protein environment there (**Fig. 3b**). Instead of being exposed to FnIII-1'

‘top’ loops the DILP5 faces here only a very small patch on the side β-strands of this domain; the main contact here is formed by double hydrogen bond of AsnB1 to CO of Ser880 and NH of Ser881. Shrinking of the down site 1b results also from the proximity of DILP5 hormones in site 1a and site 2’. The interface between DILPs is maintained by AspB12, MetB13, ArgB15 and ValB16 from hormone in site 1a, and SerB2, ArgB4, AsnA12-CysA14 region from site 2’ DILP5. There is an interesting convergence of B1-B4 chains from site 1a and site 2’ DILPs on the Pro880-Pro881 patch of the FnIII-1’ domain, which serves as hydrogen bonds centre for both B1/B1’ Asn side chains (**Fig. 4d)**. The 827-842 loop – important in site 1b’ - does not have any structurally discriminatory role in site 1b as this part of the FnIII-1’ domain is away from the hormone binding site.

The site 2’ bound DILP5 uses mostly B-chain α–helix residues MetB11(ValB12), AspB12(GluB13), ValB16(LeuB17), AlaB17(ValB18)), as well as AsnB1, and A-chain PheA16(LeuA13) and ArgA20(ArgA17) to interact with FnIII-1’ β-strands (e.g. Ser815, Met882, Met888, Val889). Importantly, the site 2’ hormone is expanded and supported by the dmIR-ECD specific Ala1168-Ser1189 ledge-like loop, where its central short Ile1173-Thr1181 helix runs ca. 45° below the B8-B18 DILP5 α-helix (**Fig. 3d**). There seems to be a lack of very specific helix-helix interactions here, with the closest contact being between the Phe1183 benzene ring which props up the hormone’s MetB11 region.

Interestingly, site 2’ DILP5 uses again B-chain α-helix:β-strands protein-protein interaction motif, observed previously in its complex with Imp-L2 binding protein (Roed *et* al, 2018). However, despite the re-occurrence of similar DILP5 side chains on such interface (MetB13, ValB16, AlaB17, PheA16) its nature in dmIR complex is different, as the B-helix runs almost parallel to FnII1-1’ β-strands (**Fig. 3c**), while it is perpendicular to the direction of the β-sheet in Imp-L2.

It should be noted that the A1-A3 part of the A-chain in site 2’ DILP5 becomes part of a long A1-A12 α-helix, unique for DILPs in this complex . This brings the A-chain N-terminus close (within possible hydrogen bond distances) to the C-terminus of the B-chain (B24Ser) (**Fig. 3c-d**). Interestingly, such helical conformation of A1-A4 does not result from any particular steric requirements as it faces open solvent space. It may be speculated that this is an overall effect of the proximity of the Ile1173-Thr1181 ledge’s α-helix and B20-B24 β-strand, in order to keep the DILP5 molecule firmly compact above this site 2’ dmIR-unique ledge region.

The role of Ala594-Asn615 (Cys259-280His) CR-domain loop.

Although the CR domains of the hIR/hIGF-1R play similar ligand-cavity enclosing role in both sites 1a and 1a', there is a specific rearrangement and length of the Ala594-Asn615 (Cys259-His280) loop in the dmIR-ECD. It has a relatively broad conformation in the hIR/hIGF-1R, leaning more outside of the receptor and bound hormones, and in the hIGF-1R it points away from the C-domain of the hIGF-1 hormone. This loop is slightly longer in the dmIR, but – importantly – it is reconfigured into a narrow β-hairpin that points directly into the DIPL5 binding cavity: the space that would be occupied by the C-domain of single-chain insulin-like family of hormones (**Fig. 3e**, **SI Fig. 5**). The space-occluding role of this loop can be amplified further by the N-glycosylation at Asn606, traces of which are suggested by the cryoEM map. It also seems that the firm position of the Ala594-Asn615 loop is reinforced by the hydrogen bonds of its central Asn606 to DILP5 ArgA3, and also contribution of loop's Phe603 to the DILP5 MetB25-binding hydrophobic cavity.

Conformational ranges of the dynamic and static protomers.

Direct structural comparisons of known human and mice IRs/IGF-1R are quite feasible due to the high similarity of their primary-to-quaternary structures. However, the evaluation of the dmIR-ECD in the context of human receptors is more complex, despite their overall similar organisation. Therefore, we selected several reference dmIR-ECD Cα sites that are quite structurally - and frequently also sequence - hIR-equivalents, hence they can serve as relative 'invariant' IRs structural pivots, facilitating easier projections of the dmIR onto human/mice IRs and IGF-1R (see **SI Table 2**).

In general, the mutual tolerance of site 1 and site 2'-bound insulins by the down-arm Λ protomer does not require very special/radical angular movements of the L1-CR-L2 domains. Instead, it is achieved by conformational changes that are within the ranges observed for the static and dynamic h/mIR protomers (**Fig. 5**). The trajectory movement of the L1-CR-L2 down Λ arm in the dmIR-ECD - upon simultaneous accommodation of two DILP5 hormones in site 1 down and site 2' - is not simply upward, but it combines up- and side-movements of these parts of the dmIR. Subsequently, the dmIR specific three hormones (two-close 'down', one 'up') quaternary assembly is easily attained by structural changes that

remains well within the broad spectrum of h/mIR individual conformers (Forbes, 2023) and the whole receptors. and their movements (see **SI Table 2 Summary, SI Fig. 6**).

The impact of insulin binding on closeness of membrane-proximal FnIII-3 domains; receptor activation.

The translation of binding of DILP5 to three dmIR-ECD sites results in rather a more screw-like and asymmetric approach of FnIII-3 domains. The C-termini of FnIII-3/FnIII-3' domains are 111 Å apart in the apo-hIR form (e.g. PDB ZXB) to becoming ~20 Å close is some 1-3 insulin bound hIR conformers (e.g. 6HN5+6HN5, 7pg0-7pg4), and ~37-40 A in T-shaped 4 insulins/IR complexes. In the dmIR-ECD this distance (measured at Val1283(Val905 (or Val886 in 6HN4)) is ~27 Å, with the FnIII-3/FnIII-3' domains being vertically shifted against each other by ~6-10 Å (depending on sites of reference in FnIII-3).

Modelling of DILP1-4 binding to the dmIR.

To get an approximate insight into DILP-type specific binding to dmIR, models of DILP1-4 have been superimposed on DILP5 in dmIR-ECD site1/1' and 2' (see Methods). Although the B/A-chains cores of DILPs should remain relatively structurally invariant they show large variations in the length of A-chain N- and C-termini and B-chain N-termini **(SI Fig. 1**). It seems that binding of DILPs to down sites 1a can be envisaged without any other new, special steric hindrances; the extensions of DILPs A-chains (both N- and C-termini) and B-chain C-termini may be accommodated in there without large structural rearrangements of dmIR domains **(Fig. 6a).** These extra DILPs chains extending peptides can also fit site 2' after only moderate structural alterations as they can point into open, not dmIR-occluded spaces **(Fig. 6b**). However, this seems to be different for longer N-termini of the B-chains (e.g. in DILP1 and 7). In site 2' they may have to thread in-between the hormones in site 1-2' and surface of the FnIII-1' domain; this may generate some particular DILPs' sequence-dependent unfavourable interactions that may weaken formation of site 2'. As the direction of B1-B6 chains of DILP5 in site 1 and site 2' converge here on the Pro880-Pro881 region of the FnIII-1', their further simple straight extensions would clash with this domain. Similarly, the fitting of long B-chain N-termini of DILP1/7 into the upper site 1b' of the static protomer can present a structural challenge as they have to bypass the steric hindrance of the 827-842 FnIII-1 loop (**Fig. 6c**).

DISCUSSION

The conservation of the insulin/IGFs signalling axis (IIS) in the animal kingdom - postulated by a wealth of biochemical records - is supported here for the first time by the structural evidences at the insulin-like receptor level. Here we show that despite a large evolutionary insects-humans gap the molecular bases and principles of insulin:IR (and to some extent hIGF1:IGF-1R) coupling are preserved on an astonishing and remarkable level. This work allows to expand the known conservation of the IIS observed in the similar 3-D nature of the human and Dm insulins onto (i) analogous organisation and similar 3-D folds of the ECDs of their receptors (including IGF-1R), and – likely - their TKs (Pettruzzelli *et* al, 1986), (ii) similar nature of site 1/1' and site 2' hormone:IR coupling, and (iii) parallel blueprints of the overall quaternary conformations of their hormone:IR complexes, where the dmIR-ECD:DILP5 complex falls well within the spectrum of structures observed for the hIR and hIGF-1R.

However, the dmIR-ECD possesses a few Dm-specific signatures. Here, the Ala1168-Ser1189 helix-containing loop - longer than its Ala785-Ser796 human homologue - provides a supporting ledge for the site 2'-bound DILP5 making this element of the FnIII-2 domain an integral a part of this hormone binding site. This FnIII-2' domain loop acts synergistically with -the Lys884(Pro536)-Gly886(Pro549) FnIII-1' domain loop, which - being shorter than in h/mIR/hIGF-1R - minimises the steric hindrance around this novel site 2' that is required for the simultaneous accommodation of spatially adjacent and in contacts site 1/site 2'-bound hormones. These features contribute likely towards an overall better stability of such arrangement of these hormones', unseen in human insulin:IR and IGF-1R complexes. It is also interesting to note the variability of other FnIII-1 loops: (i) Thr827-Ile847 insert into human Pro495-Tyr492 loop region that may obstruct escape of longer B-chain N-termini, and (ii) a shortening of dmIR Ala907(570Val)-Thr913(579Tyr) loop that liberates more space for B-chain N-terminus. It is tempting to speculate that the long Thr827-Ile847 loop acts as a 'gatekeeper' which discriminates between DILPs with shorter or longer B-chain N-termini, thwarting – for example – an 'easy' DILP1 or DILP7 site 1' up binding mode, restricting (potentially) dmIR:DILP1 complex to two lower arm-like conformation, with a very specific signalling outcome. The variations of the dmIR loops open possibilities for this single receptor to assimilate – with different affinities - six-seven different DILPs with their variable A and B-chain termini, and subsequently to acquire different quaternary structures with DILP-specific/biased signalling outcomes.

The other functionally important structural feature of the dmIR is the reshaped - and slightly longer than in the hIR - Ala594-615Asn (Cys259-280His) CR-domain loop which may prevent binding of any insulin-like hormone with a significant C-domain (e.g. IGF-1). Indeed, the K_d for high affinity site 1 for hIGF-1 is 7780 times lower than for DILP5 C4 (5913(+/-32) and 0.76 (+/-0.16) nM, respectively) (Sajid *et al,*2011). This K_d is also lower – but much less - for IGF-2: 30(+/-6) nM- indicating that the IGF-2 four amino acids shorter than in IGF-1 C-domain may be accommodated easier by this CR loop. It is puzzling whether such a tremendous loss of dmIR binding by IGF-1results entirely from the steric clash with the CR loop, or whether it also prevents the reported threading of the α–CT segment through C-domain containing loop of this hormone (Xu *et al,* 2018). Human insulin dmIR K_d of ~60 nM (Sajid *et* al, 2011) - in the broad range of IGF-2 binding – can represent the impact and importance of species-particular amino acid sequence if the overall 3-D structural scaffold of the hormone is maintained in the process of speciation. Therefore, the Ala594-615Asn CR loop may be of evolutionary importance, as its less pronounced structural role in mammalian IR/IGF-1R-like receptors results in insulin-like RTKs (human/mice etc.) capable of binding a wider variety of two- or single-chain ILP-like hormones. This would allow both the maintenance/use of a relatively narrow population of insulin-like hormones with simultaneous assurance of a broad spectrum of signal transductions through the hetero-dimerised isoforms of their IRs, e.g. the IR-A/IR-B and IR-A/IGF-1R hybrids in humans. Therefore, it can be envisaged that the selection of only one TK receptor in *Drosophila* led to the co-development of seven, C-domain free DILPs to assure the necessary complexity of IIS axis in insects life cycle.

The less symmetrical assembly of the transmembrane-proximal FnIII-3 domains in the dmIR:DILP5 complex may be considered as a part of more convoluted downstream translation of site 1/1' and 2' hormone-binding into not only a 'getting together' binary coupling of the respective cytoplasmic TKs, but their much more complex translational/rotational (pistons-like) 3-D rearrangements. Such signal transduction would allow fine, sequential and more complex phosphorylation activation patterns of the kinases, hence different and modulated (biased) intra-cellular responses.

The occurrence of an asymmetrical *T*-like shape of the dmIR-ECD:DILP5 complex at the supraphysiological concentration of this hormone may seem surprising in the context of mainly symmetrical T-shaped hIR:insulin complexes observed at the saturated levels of the hormone. However, the structural asymmetry of hormone;receptor complex observed in this

report sheds also more light on the mechanism of negative cooperativity in this family of receptors (De Meyts *et al*. 1973), which has been postulated to be linked to the induction of ligand-induced receptor asymmetry (De Meyts, 2015)). When measured kinetically by the classical assay of ligand-accelerated dissociation of a bound radioligand, the dose-response-curve for insulin dissociation is bell-shaped with disappearance of the acceleration at concentrations over 100 nM (De Meyts, 1973, Kiselyov *et al,* 2009). In contrast, both the hIGF-1R at the hIGF-1 supraphysiological level (Kiselyov *et al,* 2009), and the dmIR at the excess DILP5 (Sajid *et* al, 2011), maintain the negative cooperativity, showing indeed its correlation with the asymmetrical configuration of their complexes. This is also supported by the data with IRs and IGF-1Rs with modified α–CT segments (Li *et* al, 2022). It must be noted though, that the DILP5:dmIr-ECD complex described here is based on a lower affinity ectodomain that lacks any FnIII-1 domains joining – e.g. Leu-zipper-like tags – which may play a role in trapping this part of the receptor in three-only hormone conformation. Therefore, whether such hormone:receptor asymmetry is species-specific conformational limitation/barrier of dmIR, or whether it may be pushed further into the symmetrical T-state by other DILPs in the negative cooperativity-free process, requires further studies.

The DILP5:dmIR-ECD structure also opens a new venue for specifically dmIR engineered – and phenotypically validated - transgenic *Drosophila* flies as models for particular human diseases. Here, for example, our results provide a rational explanation of the impact of the recently reported Tyr902Cys dmIR missense mutation that yields temperature-sensitive flies with broad metabolic effects, making this mutant a good Type 2 Diabetes model (Banzai & Nishimura, 2023). Tyr902 is at the centre of a hydrophobic core at the base of 867-877 loop that spans inter-protomer FnIII-1 domains *via* Cys873-Cys873' disulphide bridge. The Tyr902Cys mutation can destabilise this region (important for the dimeric state of the dmIR) by an abnormal intra-protomer Cys902-Cys873 disulphide coupling, as suggested by Banzai & Nishimura (2023) (**SI Fig. 7**), leading to low folding efficiency of dmIR hence its reduced bioavailability. Moreover, another temperature sensitive and metabolic phenotype Val811Asp mutation (Banzai & Nishimura, 2023) can also be explained by the destabilisation of the Val811 hydrophobic cavity, of which the immediate proximity to Tyr902-containing β-strand seems to be crucial for the proper maintenance and formation of the inter-protomer Cys873- Cys873' bridge. Therefore, a similar, but weaker than Tyr902Cys-like mutations effect can be expected by the disturbance of the Val811 site.

In summary, this report provides the first evidence of the structural conservation of the IIS axis at the IR level, underpinning the wealth of biochemical and cellular data of close functional mimicry of mammalian/human insulin signalling in non-vertebrate Metazoa. The dmIR-specific structural signatures contribute also to a better understanding of *Drosophila* as a model for human pathologies and aging, highlighting also further dmIR-targets for more rational genetic and cellular manipulation of this system.

METHODS

Production of *Drosophila* insulin receptor ectodomain expressing baculovirus

A vector encoding a codon optimized version of Drosophila insulin receptor (Uniprot ID: P09208) ectodomain (dmIR ecto) was a gift from Nikolaj Kulahin Roed (Novo Nordisk). The coding sequence beginning with the native signal sequence of dIR was predicted using the SignalP web service (Teufel *et al*, 2022). DNA encoding the amino acids 292-1309 of dmIR was subcloned into the vector pBAC™4x-1 DNA (Novagen) downstream of the p10 promoter behind an IMP-L2 secretion peptide with a C-terminal StrepII-tag. Bacmid (gift from Ian M. Jones, University of Reading) was purified from *E. coli* and digested with BsuI (Zhao *et al*, 2003). V1 baculovirus was produced by mixing linearized bacmid with purified baculotransfer vector and FugeneHD transfection reagent (Promega) and incubated with adherent Sf9 cells (Invitrogen) at ratio of 3:4:12 bacmid:vector:FugeneHD in a 6-well plate (0.75 microgram : 2 microgram : 6 microlitre per 2 mL well). V1 to V2 baculovirus amplification was performed in Sf9 suspension culture, and the GFP present in the baculotransfer vector, upstream of a polyhedrin promoter, was used to determine optimum amplification before harvest (typically >90% cells fluorescent).

Expression and purification of Drosophila insulin receptor ecto-domain

The dmIR ecto domain was expressed in Sf9 cells infected with V2 baculovirus at a MOI>1 and infection followed using the GFP marker to determine optimum time for harvest (typically 72 h, with >90% cells fluorescent). Conditioned media (2.4 L) was cleared by centrifugation at 500 x *g* for 20 mins at 4 °C followed by a second clearing of debris by centrifugation at 5000 x *g* for 30 min at 4 °C. The cleared conditioned tangential flow media was placed onto a 30 kDa cut-off filtration (TFF) column (Repligen, S02-E030-05-N, surface area 790 cm^2). The media was concentrated 10-fold by placing the feed tube in the media and applying 12 PSI transmembrane pressure (TMP) and 20 mL/minute flux rate. The retentate was diafiltrated by placing the feed tube in the purification buffer until at least a 10-fold

volume of the purification buffer was consumed. The diafiltrate was incubated with a CaCl2 and NiCl2 solution stirring at RT for 30 minutes and cleared of debris by centrifugation at 18,000 x *g* for 60 minutes at 4 °C. Samples were passed through Strep Trap HP 1 mL column (Cytiva), washed with the purification buffer and eluted with 2.5 mM Desthiobiotin. The eluent was pooled and concentrated to a volume of ~0.5 mL with a 30-kDa Vivaspin concentrator (GE Healthcare) and further purified by size-exclusion chromatography (SEC) with a Superdex S200 10/300 column (Cytiva) in SEC buffer (20 mM HEPES, 200 mM NaCl, pH 7.4). dmIR ecto domain containing fractions were concentrated to 2 mg/mL with a 30-kDa Vivaspin concentrator. Purity of samples was assessed by SDS-and Native-PAGE (**SI Fig. 8**).

Titration of DILP-5 hormone into *Drosophila* IR *ecto* domain has been carried out using MicroCal iTC200 instrument (Malvern Instruments). Titration data obtained from nineteen 2 uL injections of DILP5 11607 g/mol (100 uM) into dIR*ecto* 233538 g/mol (5.3 uM). All injections were carried out in 50 mM Tris, 150 mM NaCl, pH 7.4 buffer. Data fitting and analysis was carried out with the manufacturer's software, MicroCal PEAQ-ITC Analysis.

Cryo-electron microscopy data collection of *holo* dmIR ectodomain

holo dmIR ecto was prepared by incubating with a 5-fold molar excess of DILP5 (kindly donated by Novo Nordisk). The *holo* dmIR ecto domain was prepared on UltraAuFoil R1.2/1.3 gold support grids (Quantifoil). 3 microliters of sample was applied to glow-discharged grids, blotted for 2s with -10 force and vitrified by plunging into liquid ethane using the FEI Vitrobot Mark IV at 4 °C and 100% relative humidity. Micrographs were collected at the Diamond eBIC facility on Titan Krios microscope (FEI) operating at 300 kV, and equipped with K3 camera and an energy filter (Gatan) using slit width of 20 eV. Automated data collection was performed using FEI EPU software. 4858 movies were collected in super resolution mode with super resolution pixel size of 0.4145. The defocus range chosen for automatic collection was 0.5 to 4 μm.

Image processing and reconstruction.

All datasets were processed in RELION 3.1.2 (Zivanov *et al,* 2018) and Topaz 0.2.3 (Bepler *et al*, 2019). Movie frames of the *holo* dmIR ecto domain were motion corrected binning by 2 to the physical pixel size of 0.829 Å, and dose-weighted using a does per frame of 1.03 e/Å^2 using the Motioncorr2 program (Zheng 2017). CTF parameters were estimated using

CTFFIND4 (Rohu 2015). An initial round of autopicking was performed in RELION using LoG. ~1.2 million particles were extracted and subjected to several rounds of reference-free 2D classification to remove particles associated with noisy or contaminated classes resulting in 318,846 particles. 2D classes showing sharp structural features were chosen to build an initial 3D model. This initial model was then used for 3D classification. The class showing well defined structural features was then selected for 3D refinement which gave a reconstruction with a resolution of 9 Å. 1250 particles from this class were then used to train Topaz on a dataset comprising all micrographs. Following picking with Topaz using this model ~730K particles were extracted from which rounds of 2D classification and a selection for the initial model resulted in two reconstructions consistent with 'open' and 'closed' conformations of the receptor. Further rounds of 3D classification and 3D refinement (**SI Fig. 3**) resulted in areconstruction of the holo-dmIR-ECD at 3.9 Å resolution.

Model building refinement and validation

Individual domains of dmIR ectodomain were predicted using Alphafold and docked as rigid bodies into the 3.9 Å resolution CryoEM maps using UCSF Chimera's "Fit in map" function (Pettersen *et al*, 2021). Atomic model building of the DILP5 hormone was performed using the previously reported crystal structure core residues of DILP5 as an initial model, which was docked as a rigid body as described above. This initial model was modified using COOT (Emsley *et al*, 2010). Flexible model fitting was performed using ISOLDE (Croll, 2018). Real-space refinement was carried out with secondary structure restraints using Phenix (Liebschner *et al*, 2019). Model geometries were assessed with MolProbity (Williams *et al*, 2018). Structures and maps in the figures were rendered with PyMOL (http://www.pymol.org/) or ChimeraX (Pettersen *et al*, 2021). Figures were made with the ccp4mg programme (McNicholas *et al,* 2011)

Modelling of DILP1-4

Structures of DILP1-4 were homology modelled in Modeller version 9.21, using cryo-EM structure of DILP5 from its complex with DmIR. A total of 100 models were generated using the cysteine disulphide bridging constraints implemented in the software. Models with the least DOPE scores were used for further analysis. protein-protein interaction studies were performed using the Cluspro server (Kozakov *et al,* 2017). DILP5 Cα atoms 8-18 spanning B-helix in site1/1' and 2' were targets for the LSQ superposition in Coot, with the

corresponding regions in the other DILPs: DILP1 B22-B32, DILP2 B5-B15, DILP3 B7-B17 and DILP4 B7-B17.

DATA AVAILABILITY

The atomic coordinates of the DILP5:dmIR-ECD and cryoEM density map have been deposited in the Protein Data Bank and EM data bank with the accession codes 8CLS and EMD-16718.

ETHICS DECLARATION

The authors declare no competing interest.

CONTRIBUTIONS

CMV design the study, cloned and produced/characterised dmIR-ECD, and worked on CryoEM structure solution, model building/refinement, edited the manuscript, **OF** worked on protein production of dmIR-ECD, **HTJ** worked on some CryoEM aspects of this work, **TS** was responsible for the modelling work and discussions, **PDM** analysed the results and worked on the manuscript, **AMB** designed the study, analysed the results and wrote the manuscript.

ACKNOWLEDGEMENTS

We thank Maria Chechik, Oliver Bayfield and Herman Fung for the help in the initial CryoEM stages of this project, Jamie Blaza for help during the project, Tony Wild, and the Wolfson Foundation for funding the Eleanor and Guy Dodson Building and associated cryoEM facilities. We also wish to acknowledge the work of Johan Turkenburg and Sam Hart for coordinating YSBL CryoEM Facility. We are grateful to Gerd Schluckebier and Nikolaj Kulahin Roed A/S (Maaloev, Denmark) for the dmIR-ECD clone and DILP5 protein; Novo Nordisk funding of the GG Dodson Fund in York is greatly acknowledged.
CV and **AMB** were supported by MRC Grant MR/R009066/1, **OF** was funded by GG Dodson Fund in York sponsored by Novo Nordisk A/S (Maaloev, Denmark), **TS** and **AMB** were also supported by BBSRC Grant BB/W003783/1. We acknowledge Diamond for access and support of the Cryo-EM facilities at the UK national electron bio-imaging centre (eBIC), proposal BI28576, funded by the Wellcome Trust, MRC and BBSRC.

SUPPLEMENTARY INFORMATION

REFERENCES

Adams TE, Epa VC, Garrett TP, Ward CW (2000). Structure and function of the type I insulin-like growth factor receptor. *Cell Mol Life Sci* **57**: 1050-1093.

Alvino CL, McNeil KA, Ong SC, Delaine C, Booker GW, Wallace JC, Whittaker J, Forbes BE (2009). A novel approach to identify two distinct receptor binding surfaces of insulin-like growth factor II. *J Biol Chem* **284**: 7656-7664.

Banzai K, Nishimura T (2023). Isolation of a novel missense mutation in insulin receptor as a spontaneous revertant in ImpL2 mutants in Drosophila. *Development* **150**: dev201248.

Bepler T, Morin A, Bepler T, Morin A, Rapp M, Brasch J, Shapiro L, Noble AJ, Berger B (2019). Positive-unlabeled convolutional neural networks for particle picking in cryo-electron micrographs. *Nat Methods* 16, 1153–1160

Bier E (2005). Drosophila, the golden bug, emerges as a tool for human genetics. *Nat Rev Genet* **6**: 9-23.

Blyth AJ, Kirk NS, Forbes BE (2020). Understanding IGF-II action through insights into receptor binding and activation. *Cells* **9**:2276.

Brogiolo W, Stocker H, Ikeya T, Rintelen F, Fernandez R, Hafen E (2001). An evolutionarily conserved function of the Drosophila insulin receptor and insulin-like peptides in growth control. *Curr Biol* **11**: 213-221.

Brzozowski AM, Dodson EJ, Dodson GG, Murshu GN, Verma C, Turkenburg JP, de Bree FM, Dauter Z (2002) Structural origins of the functional divergence of human insulin-like growth factor-I and insulin. *Biochemistry* **41**: 9389-9397.

Chan SJ, Steiner DF (2000). Insulin through the ages: phylogeny of a growth promoting and metabolic regulatory hormone. *American Zoologist* **40**: 213-222.

Colombani J, Andersen DS, Boulan L, Boone E, Romero N, Virolle V, Texada M, Leopold P (2015). Drosophila Lgr3 couples organ growth with maturation and ensures developmental stability. *Curr Biol* **25**: 2723-2729.

Croll TI (2018). ISOLDE: a physically realistic environment for model building into low-resolution electron-density maps. *Acta Cryst* **D74**:519-530

Croll TI, Smith BJ, Margetts MB, Whittaker J, Weiss MA, Ward CW, Lawrence MC (2016). Higher-resolution structure of the human insulin receptor ectodomain: multi-modal inclusion of the insert domain. *Structure* **24:** 469-476.

De Meyts P (1994). The structural basis of insulin and insulin-like growth factor-I (IGF-I) receptor binding and negative cooperativity, and its relevance to mitogenic versus metabolic signaling. *Diabetologia* **37**: S135-S148.

De Meyts P (2004). Insulin and its receptor: structure, function and evolution. *Bioessays* **26**: 1351-1362.

De Meyts P (2015). Insulin/receptor binding: the last piece of the puzzle? *Bioessays* **37**: 389-397.

De Meyts P (2016). The insulin receptor and its signal transduction network. In: K.R. Feingold *et al.* (Eds.), *Endotext* (Internet), South Dartmouth (MA), MDtext.com Inc., 2000.

De Meyts P, Roth J, Neville DM Jr, Gavin JR III, Lesniak MA (1973). Insulin interaction with its receptors: experimental evidence for negative cooperativity. *Biochem Biophys Res Commun* **55**: 154-161.

De Meyts P, Van Obberghen E, Roth J, Wollmer A, Brandenburg D (1978). Mapping of the residues responsible for the negative cooperativity of the receptor binding region of insulin. *Nature* **273**: 504-509.

De Meyts P, Whittaker J (2002). Structural biology of insulin and IGF1 receptors: implications for drug design. *Nat Rev Drug Discov* **1**:769-783.

Denley A, Cosgrove LJ, Booker GW, Wallace JC, Forbes BE (2005). Molecular interactions of the IGF system. *Cytokine Growth Factor Rev* **16**:421-439.

Emsley P, Lohkamp B, Scott WG, Cowtan K. (2010). Features and development of Coot *Acta Crystallogr.* **D66**:486-501.

Fernandez R, Tabarini D, Azpiazu N, Frasch M, Schlessinger J (1995). The Drosophila insulin receptor homolog: a gene essential for embryonic development encodes two receptor isoforms with different signaling potential. *EMBO J* **14**:3373-3384.

Forbes BE (2023). The three-dimensional structure of insulin and its receptor. In *Hormone receptors: structures and function.* Vitamins and Hormones, Gerald Litwack, editor, Academic Press/Elsevier, in press.

Forbes BE, McCarthy P, Norton RS (2012). Insulin-like growth factor binding proteins: a structural perspective. *Front Endocrinol (Lausanne)* **3**:38.

Gauguin L, Delaine C, Alvino CL, McNeil KA, Wallace JC, Forbes BE, De Meyts P (2008). Alanine scanning of a putative receptor binding surface of insulin-like growth factor-I. *J Biol Chem* **283**: 20829-20821.

Grönke S, Clarke DF, Broughton S, Andrews TD, Partridge L (2010). Molecular evolution and functional characterization of Drosophila insulin-like peptides. *PloS Genet* **6**: e1000857.

Gutmann T, Kim KH, Grzybek M, Walz T, Coskun Ü (2018). Visualization of ligand-induced transmembrane signaling in the full-length human insulin receptor. *J Cell Biol* **217**: 1643-1649.

Gutmann T, Schäfer IB, Poojari C, Brankatsch B, Vattulainen I, Strauss M, Coskün Ü (2020). Cryo-EM structure of the complete and ligand saturated insulin receptor ectodomain. *J Cell Biol* **219**:e201907z10.

Kavran JM, McCabe JM, Byrne PO, Connacher MK, Wang Z, Ramek A, Sarabipour S, Shan Y, Shaw DE, Hristova K, Cole PA, Leahy DJ (2014). How IGF-1 activates its receptor. *eLife* **3**:1-28.

Kenyon C (2011). The first long-lived mutants: discovery of the insulin/IGF-1 pathway for ageing. *Phil Trans R Soc B* **366**: 9-16.

Kim J, Yunn N-O, Park M, Kim J, Park S, Kim Y, Noh J, Ryu SH, Cho Y (2022). Functional selectivity of insulin receptor revealed by aptamer-trapped receptor structures. *Nat Commun* **13**:6500.

Kirk NS, Chen Qi, Wu YG, Asante AL, Hu H, Espinosa JF, Martinez F, Margetts MB, Mohammed FA, Kiselyov VV, Barrett DG, Lawrence MC (2022). Activation of the human insulin receptor by non-insulin-related peptides. *Nat Commun* **13**:5695.

Kiselyov VV, Versteyhe S, Gauguin L, De Meyts, P (2009). Harmonic oscillator model of the insulin and IGF1 receptors' allosteric binding and activation. *Mol Sys Biol* **5**: 243.

Kozakov D, Hall DR, Xia B, Porter KA, Padhorny D, Yueh C, Beglov D, Vajda S. (2017) The ClusPro web server for protein-protein docking. *Nature Protocols* **12**:255-278.

Kremer LPM, Korb J, Bornberg-Bauer E (2018). Reconstructed evolution of insulin receptors in insects reveals duplications in early insects and cockroaches. *J Exp Zool (Mol Dev Evol)* **330**: 305-311.

Lawrence MC (2021). Understanding insulin and its receptor from their three-dimensional structures. *Mol Metab* **52**: 101255.

Li J, Choi E, YU H, Bai X-c (2019). Structural basis of the activation of type 1 insulin-like growth factor receptor. *Nat Commun* **10**:4567.

Li J, Park J, Mayer JP, Webb KJ, Uchikawa E, Wu J, Liu S, Zhang X, Stowell MHB, Choi E, Bai X-c (2022a). Synergistic activation of the insulin receptor via two distinct sites. *Nat Struct Mol Biol* **29**:357-368.

Li J, Wu J, Hall C, Bai X-c, Choi E (2022b). Molecular basis for the role of disulfide-linked αCTs in the activation of insulin-like growth factor 1 receptor and insulin receptor. *eLife* **11**:e811286.

Liebschner D, Afonine PV, Baker ML, Bunkókzi G, Chen VB, Croll TI, Hintze B, Hung LW, Jain S, McCoy AJ, Moriarty NW, Oeffner RD, Poon BK, Prisant MG, Read RJ, Richardson S, Richardson DC, Sammito MD, Sobolev DV, Stockwell DH, Terwilliger TC, Urzumstev AG, Videau LL, Williams CJ, Adams PD (2022). Signal 6.0 predicts all five types of signal peptides using protein language models. *Nat Biotechnol* **40**:1023-1025.

McNicholas S, Potterton E, Wilson KS, Noble ME. (2011) Presenting your structures: the CCP4mg molecular-graphics software. *Acta Crystallogr.* **D67**, 386-94.

Nagao H, Cai W, Brasil Brandao B, Wewer Albrechtsen N, Steger M, Gattu AK, Pan H, Dreyfuss JM, Wunderlich FT, Mann M, Kahn CR (2022). Leucine-973 is a crucial residue differentiating insulin and IGF-1 receptor signaling. *J Clin Invest* **22e**:161472.

Nielsen J, Brandt J, Boesen T, Hummelshoj, Slaaby R, Schluckebier G, Nissen P (2022). Structural investigations of full-length insulin receptor dynamics and signalling. *J Mol Biol* **434**:167458.

Okamoto N, Nakamori R, Murai T, Yamauchi Y, Masuda A, Nishimura T (2022). A secreted decoy of InR antagonizes insulin/IGF signaling to restrict body growth in Drosophila. *Genes & Development* **27**:87-97.

Park J, Li J, Mayer JP, Ball KA, Wu J, Hall C, Accili D, Stowell MHB, Bai X-c, Choi E (2022). Activation of the insulin receptor by an insulin mimetic peptide. *Nat Commun* **13**:5594.

Petruzzelli L, Herrera R, Garcia-Arenas R, Rosen OM (1985). Acquisition of insulin-dependent protein tyrosine kinase activity during *Drosophila* embryogenesis. *J Biol Chem* **260**: 16072-16075.

Petruzzelli L, Herrera R, Arenas-Garcia R, Fernandez R, Birnbaum MJ, Rosen OM (1986). Isolation of a Drosophila genomic sequence homologous to the kinase domain of the human insulin receptor and detection of the phosphorylated Drosophila receptor with anti-peptide antibody. *Proc Natl Acad Sci USA* **83**: 4710-4714.

Pettersen EF, Goddard TD, Huang CC, Meng EC, Couch GS, croll TI, Morris JH, Ferrin TE (2021). UCSF ChimeraX: structure visualization for researchers, educators and developers. *Protein Sci* **30**: 70-82.

Pierce SB, Costa M, Wisotskey R, Devadhar S, Homburger SA, Buchman AR, Ferguson KC, Heller J, Platt DM, Pasquinelli AA, Liu LX, Doberstein SK, Ruvkun G (2001). Regulation of DAF-2 receptor signaling by human insulin and INS-1, a member of the unusually large and diverse C. elegans insulin gene family. *Genes Dev* **15**:672-686.

Post S, Karaschuk G, Wade JD, Sajid W, De Meyts P, Tatar M. (2018). Drosophila insulin-like peptides DILP2 and DILP5 differentially stimulate cell signaling and glycogen phosphorylase to regulate longevity. *Frontiers Endocrinol (Lausanne)* **9**: 245.

Pullen RA, Lindsay DJ, Wood SP, Tickle IJ, Blundell TL, Wollmer A, Krail G, Brandenburg D, Zahn H, Gliemann G, Gammeltoft S (1976). The receptor-binding region of insulin. *Nature* **259**:369-373.

Roed NK, Viola CM, Kristensen O, Schluckebier G, Norrman M, Sajid W, Wade JD, Andersen AS, Kristensen C, Ganderton TR, Turkenburg JP, De Meyts P, Brzozowski AM (2018). Structures of insect Imp-L2 suggest an alternative strategy for regulating the bioavailability of insulin-like hormones. *Nat Commun* **9**: 3860.

Rohu A, Grigorieff (2015). NCTFFIND4: Fast and accurate defocus estimation from electron micrographs. *J Struct Biol* **192**: 216-221.

Ruan Y, Chen C, Cao Y, Garofalo RS (1995). The Drosophila insulin receptor contains a novel carboxy-terminal extension likely to play an important role in signal transduction. *J Biol Chem* **270**: 4236-4243.

Sajid W, Kulahin N, Schluckebier G, Ribel U, Henderson HR, Tatar M, Hansen BF, Svendsen AM, Kiselyov V, Norgaard P, Wahlund P-O, Brandt, J, Kohanski RA, Andersen AS, De Meyts P (2011). Structural and biological properties of the *Drosophila* insulin-like peptide 5 shows evolutionary conservation. *J Biol Chem* **286**: 661-673.

Saltiel AR (2021). Insulin signaling in health and disease. *J Clin Invest* **131**:e142241.
Scapin G, Dandey VP, Zhang Z, Prosise W, Hruza A, Kelly T, Mayhood T, Strickland T, Potter CS, Carragher B (2018). Structure of the insulin receptor-insulin complex by single-particle cryo-EM analysis. *Nature* **556**: 122-125.

Siddle K (2012). Molecular basis of signaling specificity of insulin and IGF receptors: neglected corners and recent advances. *Front Endocrinol* (Lausanne) 3:34.

Smýkal V, Pivarci M, Provazník J, Bazalová O, Jedlicka P, Luksan O, Horák A, Vanecková H, Benes V, Fiala I, Hanus R, Dolezel D (2020). Complex evolution of insect insulin receptors and homologous decoy receptors, and functional significance of their multiplicity. *Mol Biol Evol* **37**: 1775-1789.

Tatar M (2021). Aging regulated through a stability model of insulin/insulin growth factor receptor function. *Front Endocrinol (Lausanne)* **12**:649880.

Teleman AA, Ratzenböck I, Oldham S (2012). Drosophila: a model for understanding obesity and diabetes complications. *Exp Clin Endocrinol Diabetes* **120**: 184-185.

Teufel F, Arementeros JJA, Johansen AR, Gíslason MH, Pihl SI, Tsitigos KD, Winther O, Brunak S, von Hejne G, Nielsen H (2019). Macromolecular structure determination using X-rays, neutrons and electrons; recent developments in Phenix. *Acta Crystallogr.* **D75**: 861-877.

Uchikawa E, Choi E, Shang G, Yu H, Bai X-c (2019). Activation mechanism of the insulin receptor revealed by cryo-EM structure of the fully liganded receptor-ligand complex. *eLIFE* **8**:e48630.

Ugur B, Chen K, Bellen HJ (2016). Drosophila tools and assays for the study of human diseases. *Dis Model Mech* **9**:235-244.

Weis F, Menting JG, Margetts MB, Chan SJ, Xu Y, Tennagels N, Wohlhart P, Langer T, Müller CW, Dreyer MK, Lawrence MC (2018). The signalling conformation of the insulin receptor ectodomain. *Nat Commun* **9**: 4420.

Weiss M, Steiner DF, Philipson LH (2014). Insulin biosynthesis, secretion, structure, and structure-activity relationships. In: Feingold KR *et al.*, *Endotext (Internet)* South Dartmouth (MA): MDtext.com, Inc; 2000.

Williams CJ, Headd JJ, Moriarty NW, Prisant MG, Videau LL, Deis LN, Verma V, Keedy DA, Hinze BJ, Chen VB, Jain S, Lewis SM, Arendall WB 3rd, Shoeyink J, Adams PD, Lovell

SC, Richardson JS, Richardson DC (2018). MolProbity: More and better reference data for improved all-atom structure validation. *Protein Sci* **27**: 293-315.

Wu C, Huang X, Dong F, Tang W, Shi J, Lu X, Shu Q, Zhang X (2022). Cryo-EM structure shows how two IGF1 hormones bind to the human IGF1R receptor. *Biochem Biophys Res Commun* **636**: 121-124.

Xiong X, Blakeley A, Kim JH, Menting JG, Schäfer IB,, Schubert HL, Agrawal R, Gutmann T, Delaine C, Zhang YW, Artik GO, Merriman A, Eckert D, Lawrence MC, Coskün Ü, Fisher SJ, Forbes BE, Safavi-Hemami H, Hill CP, Chou H-C (2022). Symmetric and asymmetric receptor conformation continuum induced by a new insulin. *Nat Chem Biol* **18**: 511-519.

Xu Y, Kong GK-W, Menting JG, Margetts, MB, Delaine CA, Jenkin LM, Kiselyov VV, De Meyts P, Forbes BE, Lawrence MC (2018). How ligand binds to the type 1 insulin-like growth factor receptor. *Nat Commun* **9**: 821.

Xu Y, Kirk NS, Venugopal H, Margetts MB, Croll TI, Sandow JJ, Webb AI, Delaine CA, Forbes BE, Lawrence MC (2020). How IGF-II binds to the human type 1 insulin-like growth factor receptor. *Structure* **28**:786-798.

Xu Y, Margetts MB, Venugopal H, Menting JG, Kirk NS, Croll TI, Delaine C, Forbes BE, Lawrence MC (2022). How insulin-like growth factor I binds to a hybrid insulin receptor type 1 insulin-like growth factor receptor. *Structure* **30**: 1-11.

Zhang X, Yu D, Sun J, Wu Y, Gong J, Li X, Liu L, Liu S, Liu J, Wu Y, Li D, Ma Y, Han X, Zhu Y, Wu Z, Wang Y, Ouyiang Q, Wang T (2020). Visualization of ligand-bound ectodomain assembly in the full-length human IGF-1 receptor by cryo-EM single particule analysis. *Structure* **28**: 1-7.

Zhang X, Wei T, Wu C, Jiang J, Chen S, Hu Y, Lu Y, Sun D, Zhai L, Zhang J, Liu C. (2022). Cryo-EM structure reveals polymorphic ligand-bound states of IGF1R. *J Mol Biol* **434**:167536.

Zhang X, Wu C, Wei T, Lu Y, Liu C, Zhang J (2022). Cryo-EM studies of the apo states of human IGF1R. *Biochem Biophys Res Commun* **618**: 148-152.

Zhao Y, Chapman DAG, Jones IM (2003). Improving baculovirus recombination. *Nucleic Acids Res* **15**:E6-6.

Zheng SQ, Palovcak E, Armache J-P, Verba KA, Cheng Y, Agard DA (2017). MotionCor2: anisotropic correction of beam-induced motion for improved cryo-electron microscopy. *Nat Methods* **14**:331-332.

Zivanov J, Nakane T, Forsberg BO, Kimanius D, Hagen WJH, Lindhal E, Scheres SHW (2018). New tools for automated high-resolution cryo-EM structure determination in RELION-3. *eLife* **7**, e42166.

FIGURES

FIGURE 1.

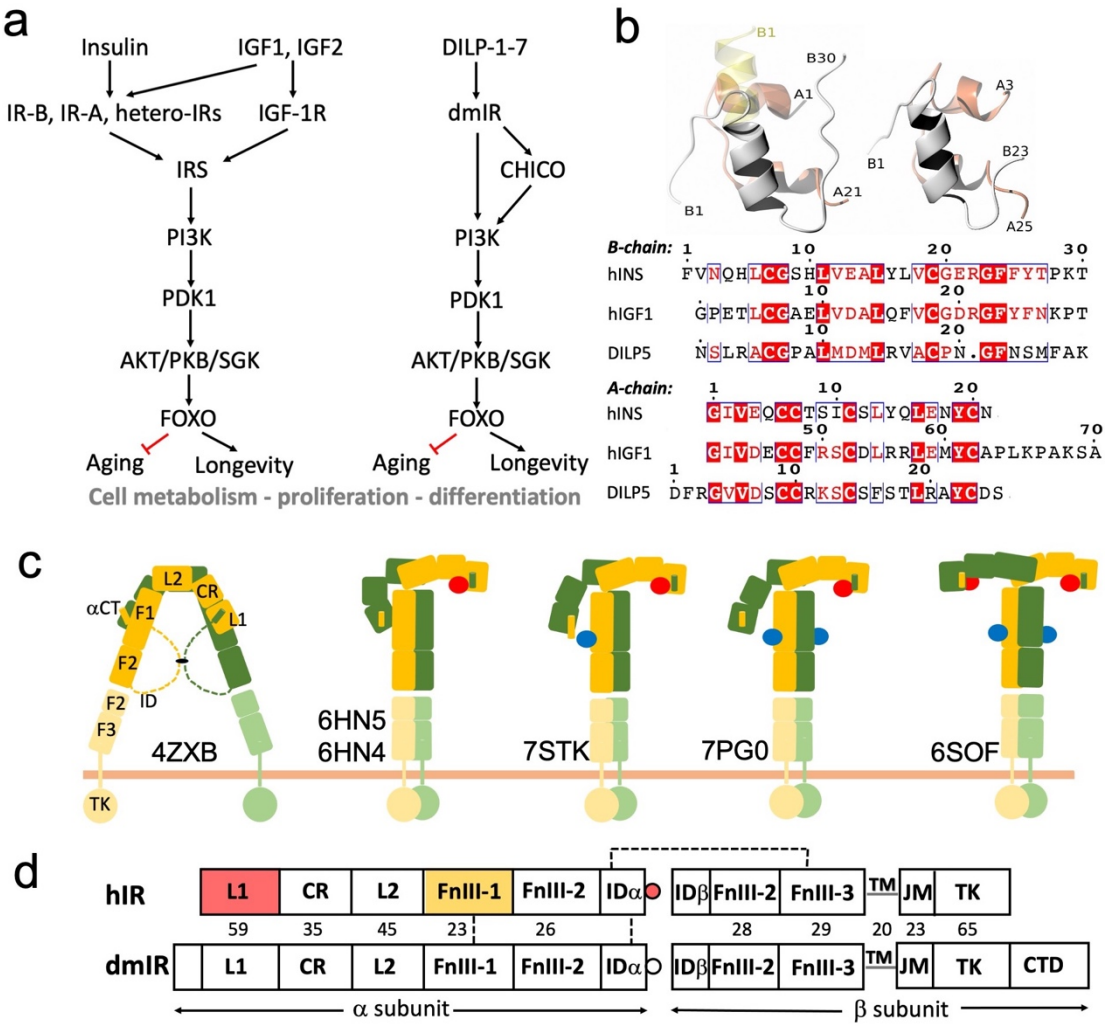

Figure 1. Summary of conservation of IIS axis in Drosophila and humans. **a** Functional homology and conservation of IIS axis in humans and *Drosophila*. **b** Structural similarity of human insulin (top left) and DILP5 (right), B-chains in grey, A-chains in coral, pale yellow in insulin – R-state of the B1-B6 N-terminus; bottom – sequence alignment of human insulin, hIGF-1 (C-domain is omitted here – not relevant for DILPs) and DILP5. **c** Schematic representation of the domain organisation and examples of some key structural conformers of hIR in the apo form (left) and in complexes with insulin, yellow/green – hIR protomers, red – insulin in site 1/1', blue – insulin in site 2/2"; PDB IDs are given for some representative structures. **d** Comparison of the domain organisation of hIR (top) and dmIR (bottom) and sequence similarity between these receptors; in red – domains involved in insulin binding site 1/1', in yellow – site 2/2'.

FIGURE 2.

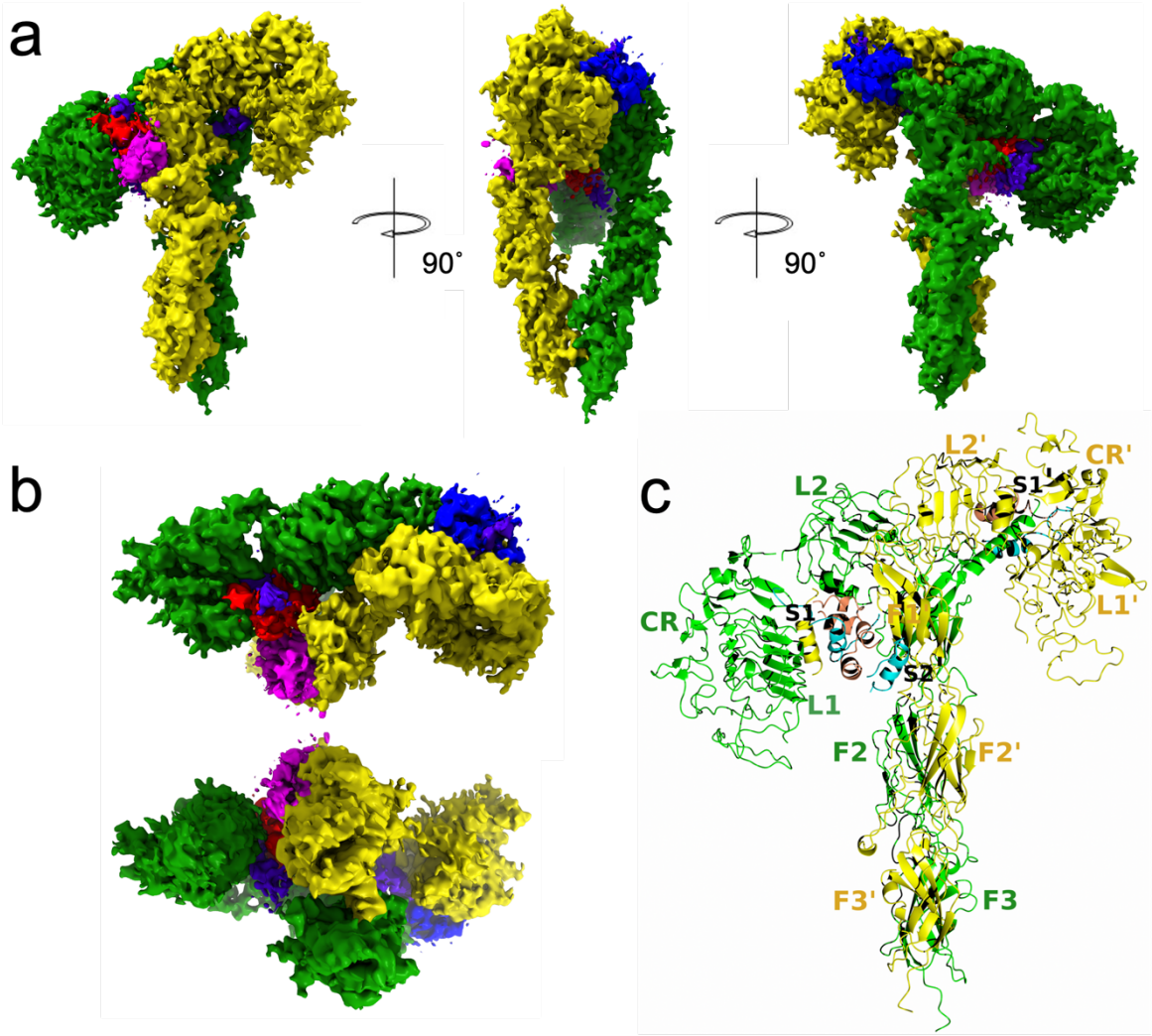

Figure 2. Overview of the cryoEM maps associated with the dmIR-ECD:DILP5 complex. **a** Side views – in green: down 'dynamic' protomer, yellow – dynamic protomer, red – DILP5 in site 1, magenta – DILP5 in site 2', blue – DILP5 in site 1', dark blue in site 1 – aCT segment. **b** top – top view of the dmIR-ECD, bottom – the view from the end of the FnIII-3/3' domains. **c** Ribbon representation of the dmIR-ECD:DILP5 complex, domains indicated by abbreviated notation, dynamic protomer in green, static protomer in yellow, DILP5 B-chains in blue, A-chains in coral. S1/1', S2' – DILP5 binding sites 1/1' and 2'.

FIGURE 3.

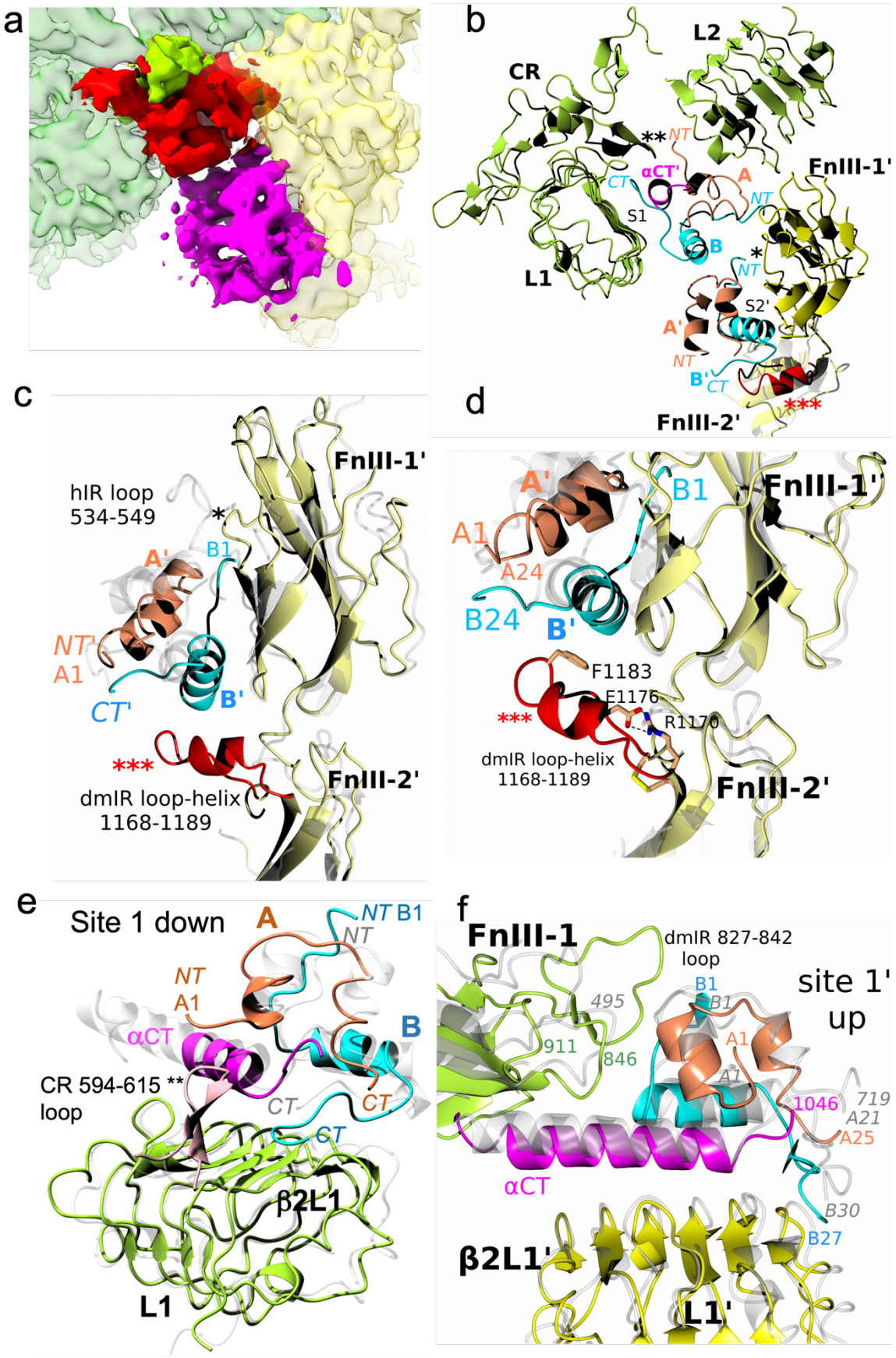
a
b
L2
CR
**
NT
αCT'
A
CT
NT
FnIII-1'
S1
B
*
NT
L1
S2'
A'
NT
B'
CT
***
FnIII-2'
c
FnIII-1'
hIR loop
534-549
*
A'
B1
NT'
A1
CT'
B'
***
FnIII-2'
dmIR loop-helix
1168-1189
d
A'
B1
FnIII-1'
A1
A24
B24
B'
F1183
E1176
***
R1170
dmIR loop-helix
1168-1189
FnIII-2'
e
Site 1 down
A
NT B1
NT
NT
A1
αCT
B
CR 594-615 **
loop
CT
CT
CT
β2L1
L1
f
FnIII-1
dmIR 827-842
loop
B1
B1
site 1'
up
495
911
846
A1
A1
1046
719
A21
A25
αCT
B30
B27
β2L1'
L1'

Figure 3. DILP5:dmIR-ECD binding sites. a cryoEM map associated with site 1 and 2' DILP5 binding; dynamic protomer in light green, static – in yellow, site 1 bound DILP5 in red, in site 2' – in magenta, α–CT' segment in bright green. **b** Ribbon representation of site 1-site 2' DILP5 binding regions; dynamic/arm-down protomer in green; static protomer in dark yellow, DILP5 B-chains in blue, A-chains in coral, α–CT' segment in magenta, human insulin and hIR in light grey, (*) – FnIII-1' Lys884-Gly886 loop, (**) - CR Ala594-615Asn loop, (*** red) – FnIII-2' 1168Ala-1189Ser ledge helix-containing loop. **c** Site 2' in dmIR-ECD – colour coding as in **b**. **d** A close-up on site 2' in dmIR-ECD showing the DILP5 supporting ledge from FnIII-2' domain and HBs (dashed lines) that stabilise this region; colour coding as in **b**, N atoms in blue, O – in red. **e – f** DILP5 site 1 down and site 1' up binding; colour coding as above; numbering in italic grey refers to hIR.

FIGURE 4.

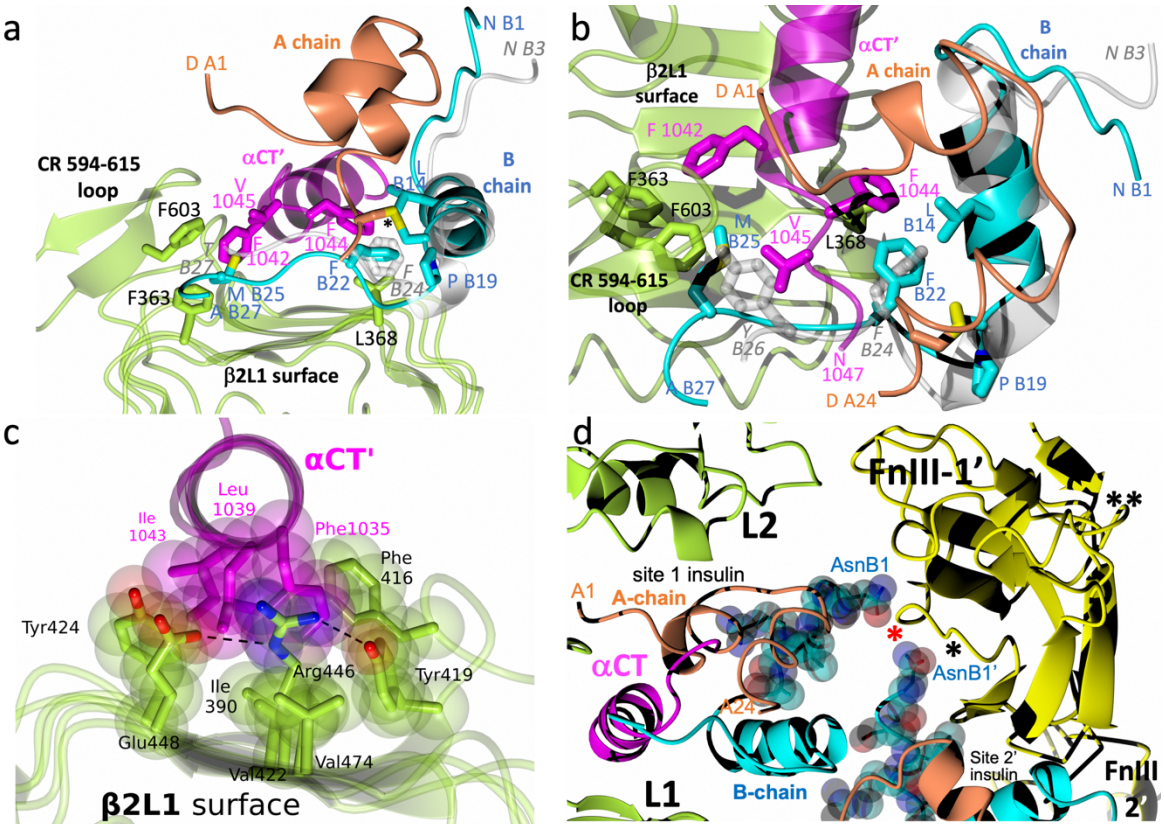

Figure 4. Conservation of some Drosophila-humans key interactions in site 1 and arrangement of DILP5 B-chains N-termini in site 1 and 2'. a-b 'side' and 'top' views of DILP5 in site 1 with some key hormone:dmIR-ECD interactions; (*) denotes A23-B18 DILP5 disulphide, colour coding as in Figure 3., human insulin (from PDB 6HN5) in grey. **c** Examples of conservation of tethering of the α–CT segment into L1-β2 surface of the L1 domain (site 1a); L1 domain and its side chains in green, α–CT segment in magenta; oxygen atoms in red, nitrogen in blue, HBs in dashed lines, van der Waals spheres for the sidechains are shown. **d** Convergence of DILP5s N-termini of the B1-B6 chains on Pro880Pro881 region (red star) of the FnIII-1' domain; B1-B5 atoms are also depicted as van der Waals spheres; 884-886 and insert 827-842 loops indicated by * and **, respectively; chains/protein colour code as in figure 3; single amino acids code was used in **a-b** for image clarity.

FIGURE 5.

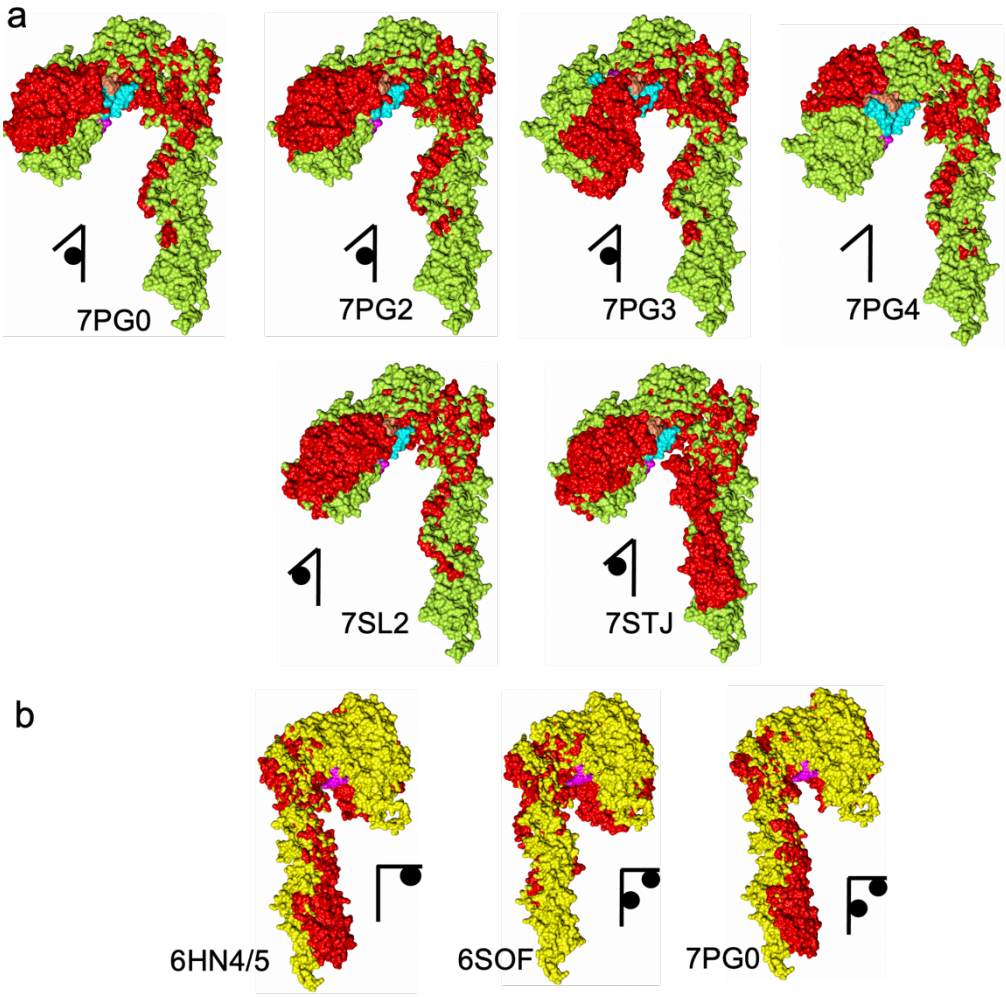

Figure 5. Superposition of dmIR-ECD dynamic and static protomers on representative human homologues. dmIR-ECD static protomers **(a)** in in green and static (**b**) (in yellow), human protomers in red with respective PDB IDs; DILP5 B-chain in blue, A-chain in coral; α-CT in magenta; black diagrams depict the number of insulins/protomer and site of binding. All protomers were superimposed in Coot (Emsley *et al*, 2010) LSQ option on Cα atoms of FnIII-1 domains: Ala807-Ans925 in dmIR on Glu471-Asp591 in hIR. The 827-847 and 881-887 loops in dmIR-ECD were removed prior to the superposition to minimise their potentially misleading bias in the superposition of the 'core' folds of the selected FnIII-1 domains.

FIGURE 6.

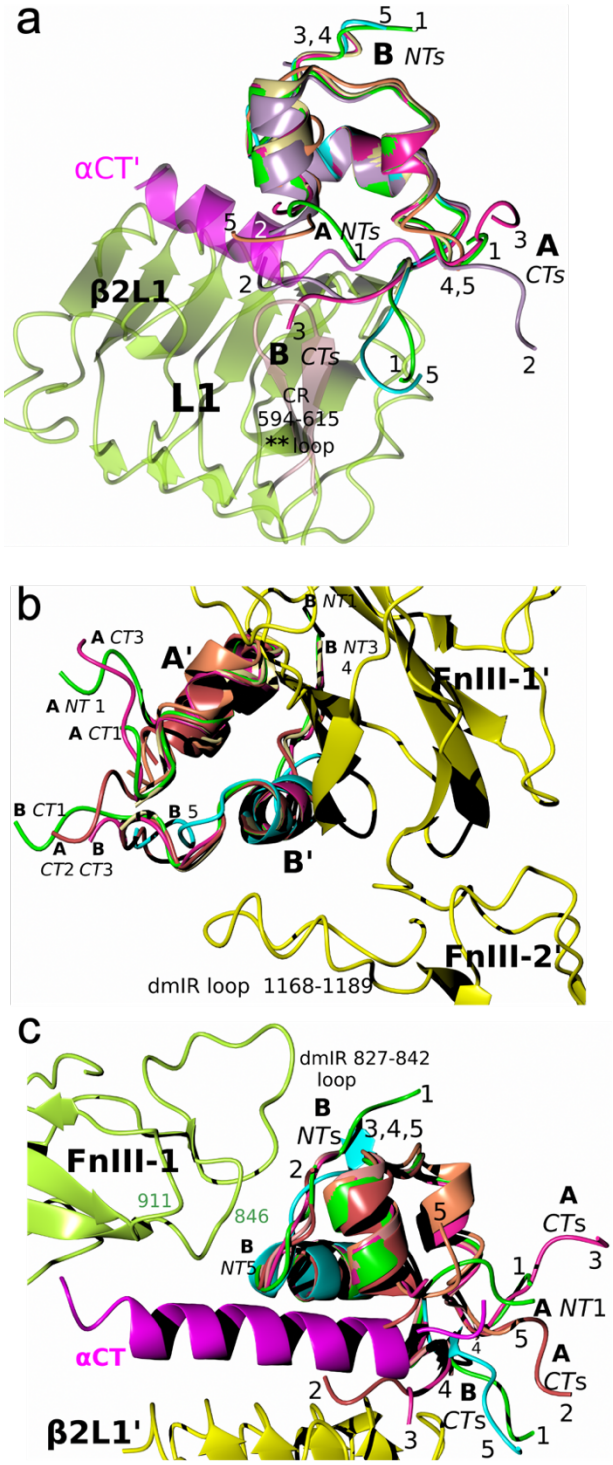

Figure 6. Models of free DILP1-4 superimposed on DILP5:dmIR-ECD structure.
a site 1a, **b** site 2' and **c** site 1' up. DILP5:dmIR-ECD colour coding as in **Fig. 3-4**; DILP1 – lime green, DILP2 – crimson, DILP3 – deep pink, DILP4 – gold; NTs-CTs indicate the N- and C-termini of respective chains, numbers correspond to DILP's type; numbers correspond to the particular DILP (e.g. 1 – DILP1).